Winter 11-30-2015

Side-Chain Boron Difluoride Formazanate Polymers via Ring-Opening Metathesis Polymerization

Samantha Novoa

Joseph A. Paquette

Stephanie M. Barbon

Ryan R. Maar

Joe Gilroy
jgilroy5@uwo.ca

Journal of Materials Chemistry C

ARTICLE

Side-Chain Boron Difluoride Formazanate Polymers via Ring-Opening Metathesis Polymerization

Received 00th January 20xx,
Accepted 00th January 20xx

DOI: 10.1039/x0xx00000x

www.rsc.org/

Samantha Novoa, Joseph A. Paquette, Stephanie M. Barbon, Ryan R. Maar and Joe B. Gilroy*

The synthesis, characterization, and ring-opening methathesis polymerization (ROMP) of a novel norbornene-based boron difluoride (BF_2) formazante monomer are described in detail. The polymerization studies confirmed ROMP to occur in the presence of BF_2 formazanates, and also demonstrated the controlled nature of the polymerization. The polymers retained many of the unique characteristics of the monomers in dichloromethane, including absorption and emission at maximum wavelengths of 518 and 645 nm, large Stoke's shifts (υ_{ST} = 127 nm, 3,800 cm^{-1}), and the ability to act as electron reservoirs to form borataverdazyl-based poly(radical anions) (E°_{red1} = –0.95 V). Furthermore, the results described in this paper demonstrate the potential of these and related polymers based on BF_2 formazanates as redox-active, light-harvesting materials.

Introduction

The incorporation of main-group elements into π-conjugated materials has proved to be an efficient strategy for the modification of their charge carrier mobility, spectroscopic characteristics, and redox activity.[1] Main-chain[2] (*e.g.*, **1**, **2**) and side-chain[3] (*e.g.*, **3**, **4**) polymers incorporating boron are an intriguing class of polymers, although their development has been relatively slow compared to those based on other main group elements (*e.g.*, S, Si, and P).[4]

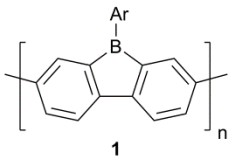

1

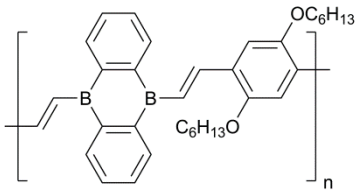

2

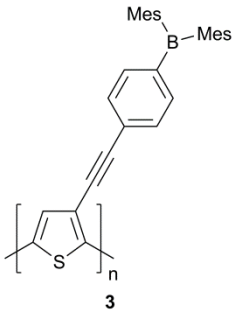

3

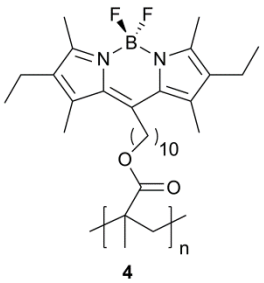

4

Formazanate ligands **5**,[5,6] derived from formazans **6**,[7] are nitrogen-rich analogs of β-diketiminates **7**.[8] BF_2 formazanate complexes have previously been shown to act as electron acceptors[5b] and their spectroscopic properties have been tuned through variation of the degree of π-conjugation[5e] and the donor/acceptor properties of their nitrogen- and carbon-bound substituents.[5c, 5d] More recently, this promising class of functional molecular materials has been exploited as contrast agents for the fluorescence imaging of the cytoplasm of mouse fibroblast cells,[5h] as efficient electrochemiluminescent (ECL) emitters,[9] and as precursors to unusual B(I)-carbenoid intermediates.[5g]

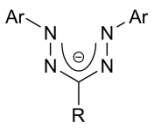

5

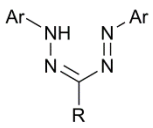

6

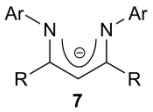

7

While rapid progress has been made in the development of molecular BF_2 formazanates, they have not been incorporated into polymer scaffolds. The realization of polymerization methods tolerant to BF_2 formazanates would allow for their unique properties to be combined with the processability of polymers. Herein, we describe the synthesis and characterization of a norbornene-containing BF_2 formazanate monomer and explore its ring-opening metathesis polymerization (ROMP) behaviour with a view of developing a class of redox-active macromolecules that may ultimately show utility as light-harvesting materials.

Department of Chemistry and the Centre for Advanced Materials and Biomaterials Research (CAMBR), The University of Western Ontario, London, Ontario, Canada, N6A 5B7.

Electronic Supplementary Information (ESI) available: [NMR spectra, TGA and DSC data, and addition cyclic voltammograms]. See DOI: 10.1039/x0xx00000x

Experimental section

General considerations

Unless otherwise stated, all reactions were carried out under a nitrogen atmosphere using standard Schlenk techniques. Solvents were obtained from Caledon Laboratories, dried using an Innovative Technologies Inc. solvent purification system, collected under vacuum, and stored under a nitrogen atmosphere over 4 Å molecular sieves. All other reagents were purchased from Sigma Aldrich or Alfa Aesar and used as received. 4-(bicyclo[2.2.1]hept-5-en-2-yl)benzaldehyde was synthesized using a published procedure.[10] NMR spectra were recorded on 400 MHz (^{1}H: 399.8 MHz, ^{11}B: 128.3 MHz, ^{19}F: 376.1 MHz) of 600 MHz (^{13}C: 150.7 MHz) Varian INOVA spectrometers. Spectra were referenced to residual $CHCl_3$ 7.27 ppm (^{1}H NMR), and $CDCl_3$ at 77.0 ppm (^{13}C NMR). ^{11}B spectra were referenced internally to BF_3•OEt_2 at 0 ppm. ^{19}F spectra were referenced internally to $CFCl_3$ at 0 ppm. Mass spectra were recorded in positive-ion mode using a Finnigan MAT 8200 spectrometer. Infrared spectra were recorded using a Bruker Vector33 spectrometer.

Absorption and Emission Spectroscopy

Solution phase UV-Vis absorption spectra were recorded using a Cary 300 Scan instrument using standard quartz cells (1 cm path length) with a scan range of 250 to 800 nm. Molar extinction coefficients were determined from the slope of a plot of absorbance against concentration using four solutions with known concentrations. Thin-film absorption spectra were recorded for films prepared by spin coating polymer **12** onto glass from a 25 mg mL^{-1} solution in chlorobenzene. Solution phase emission spectra were recorded using a QM–4 SE spectrofluorometer equipped with double excitation and emission monochromators from Photon Technology International (5 nm slit width, 0.5 nm step size). Excitation wavelengths were chosen based on absorption maxima from the respective UV-Vis absorption spectrum in the same solvent. Data were corrected for wavelength-dependent detector sensitivity (Fig. S1) and quantum yields were determined relative to ruthenium tris(bipyridine) hexafluorophosphate[11] by methods described by Fery-Forgues and co-workers.[12]

X-ray Crystallography

Single crystals for X-ray diffraction studies of monomer **11** were grown by vapour diffusion of hexanes into a saturated CH_2Cl_2 solution. The sample was mounted on a MiTeGen polyimide micromount with a small amount of Paratone N oil. X-ray diffraction measurements were made on a Bruker Kappa Axis Apex2 diffractometer at a temperature of 110 K. The data collection strategy was a number of ω and ϕ scans which collected data over a range of angles, 2θ. The frame integration was performed using SAINT.[13] The resulting data was scaled and absorption corrected using a multi-scan averaging of symmetry equivalent data using SADABS.[14] The structures were solved by dual space methodology using the SHELXT program.[15] All non-hydrogen atoms were obtained from the initial solution. The hydrogen atoms were introduced at idealized positions and were treated in a mixed fashion. The structural model was fit to the data using full matrix least-squares based on F^2. The calculated structure factors included corrections for anomalous dispersion from the usual tabulation. The structure was refined using the SHELXL–2014 program from the SHELXTL program package.[16] Graphic plots were produced using the Mercury crystallographic program suite. See Table 1 and CCDC 1426952 for X-ray diffraction data collection and refinement details.

Table 1 X-ray diffraction data collection and refinement details for BF_2 formazanate monomer **11**.

	11
Formula	$C_{26}H_{23}BF_2N_4$
Formula Weight (*g/mol*)	440.29
Crystal Dimensions (*mm*)	0.363 × 0.207 × 0.118
Crystal Colour and Habit	red plate
Crystal System	monoclinic
Space Group	P 2_1/n
Temperature, K	110
a, Å	14.339(6)
b, Å	9.360(3)
c, Å	17.092(7)
α,°	90
β,°	108.095(15)
γ,°	90
V, Å^3	2180.5(14)
Z	4
ρ (*g/cm*)	1.341
λ, Å, (MoKα)	0.71073
μ, (cm^{-1})	0.092
Diffractometer Type	Bruker Kappa Axis Apex2
R_{merge}	0.0511
R_1	0.0622
ωR_2	0.1425
R_1 (all data)	0.0985
ωR_2 (all data)	0.1621
GOF	1.036

$R_1 = \Sigma(|F_o| - |F_c|) / \Sigma F_o$; $\omega R_2 = [\Sigma(w(F_o^2 - F_c^2)^2) / \Sigma(\omega F_o^4)]^{½}$; GOF = $[\Sigma(\omega (F_o^2 - F_c^2)^2) / (\text{No. of reflns.} - \text{No. of params.})]^{½}$

Cyclic Voltammetry (CV)

CV experiments were performed with a Bioanalytical Systems Inc. (BASi) Epsilon potentiostat and analyzed using BASi Epsilon software. Typical electrochemical cells consisted of a three-electrode setup including a glassy carbon working electrode, platinum counter electrode, and silver *pseudo* reference electrode. Experiments were run at variable scan rates in degassed, dry CH_2Cl_2 or THF solutions of the analyte (*ca.* 1 mM) and electrolyte (0.1 M nBu$_4$NPF$_6$). Cyclic voltammograms were referenced relative to the ferrocene/ferrocenium redox couple (*ca.* 1 mM internal standard) and corrected for internal cell resistance using the BASi Epsilon software.

Gel Permeation Chromatography (GPC)

GPC experiments were conducted in chromatography grade THF at concentrations of 5 mg mL^{-1} using a Viscotek GPCmax VE 2001 GPC instrument equipped with an Agilent PolyPore

guard column (PL1113-1500) and two sequential Agilent PolyPore GPC columns packed with porous poly(styrene-*co*-divinylbenzene) particles (MW range 200–2,000,000 g mol^{-1}; PL1113-6500) regulated at a temperature of 30 °C. Signal response was measured using a Viscotek VE 3580 RI detector, and molecular weights were determined by comparison of the maximum RI response with a calibration curve (10 points, 1,500–786,000 g mol^{-1}) established using 10 monodisperse polystyrene standards purchased from Viscotek.

Thermal Analysis

Thermal degradation studies were performed using a TA Instruments Q600 SDT TGA. A sample of polymer **12** was placed in an alumina cup and heated at a rate of 10 °C min^{-1} from room temperature to 800 °C under a flow of nitrogen (100 mL min^{-1}). Glass transition temperatures were determined using Differential Scanning Calorimetry (DSC) on a TA Instruments DSC Q20. A sample of polymer **12** was placed in an aluminum Tzero pan and heated from 40 °C to 200 °C at 10 °C min^{-1} under a flow of nitrogen (50 mL min^{-1}) and cooled down to 20 °C at 10 °C min^{-1}, before the sample underwent another heating/cooling cycle. The glass transition was determined from the second heating/cooling cycle.

Synthetic methods

Preparation of norbornene-substituted hydrazone 9

In air, 4-(bicyclo[2.2.1]hept-5-en-2-yl)benzaldehyde **8** (1.50 g, 7.57 mmol) was dissolved in EtOH (10 mL) before a drop of 12 M HCl and phenyl hydrazine (0.82 g, 0.75 mL, 7.6 mmol) were added. Almost immediately, an off-white precipitate was formed and the solution was heated to 80 °C and allowed to reflux for 30 min. Upon cooling, the off-white precipitate was isolated by filtration and washed with cold ethanol (2 × 10 mL) to afford hydrazone **9**. Yield = 1.77 g, 81%. Hydrazone **9** was employed in subsequent reactions without further purification. ^{1}H NMR (399.8 MHz, $CDCl_3$): δ 7.69 (s, 1H, C*H*), 7.62–7.55 (m, 3H, aryl C*H*), 7.31–7.26 (m, 3H, aryl C*H*), 7.12 (d, $^3J_{HH}$ = 8 Hz, 2H, aryl C*H*), 6.88 (t, $^3J_{HH}$ = 7 Hz, 1H, aryl C*H*), 6.29–6.25 (m, 1H, =C*H*), 6.21–6.16 (m, 1H, =C*H*), 2.99 (br s, 1H, C*H*), 2.92 (br s, 1H, C*H*), 2.77–2.71 (m, 1H, C*H*), 1.79–1.72 (m, 1H, CH_2), 1.70–1.62 (m, 1H, CH_2), 1.59 (d, $^3J_{HH}$ = 8 Hz, 1H, CH_2), 1.48–1.43 (m, 1H, CH_2).

Preparation of norbornene-substituted formazan 10

In air, Na_2CO_3 (2.19 g, 20.6 mmol) and *n*Bu_4NBr (0.21 g, 10 mol %) were mixed with CH_2Cl_2 (60 mL) and deionized H_2O (60 mL) and the solution was left to stir in an ice bath for 15 min. Meanwhile, in a separate flask, aniline (0.60 g, 0.59 mL, 6.4 mmol) was mixed with 12 M HCl (1.6 mL, 19 mmol) in deionized H_2O (1.6 mL). This solution was cooled in an ice bath for 15 min before a cooled solution of sodium nitrite (0.51 g, 7.4 mmol) in deionized H_2O (5 mL) was added dropwise. The resulting reaction mixture, which contained diazonium salt, was allowed to stir in an ice bath for an additional 10 min. Hydrazone **9** (1.86 g, 6.46 mmol) was then added to the flask containing CH_2Cl_2/H_2O, and allowed to stir for 30 s, before the diazonium-containing solution was added dropwise. The solution turned dark red after approximately 2 min. The mixture was allowed to stir in an ice bath for an additional 60 min before the organic layer was collected and washed with deionized H_2O (3 x 50 mL), dried over $MgSO_4$, gravity filtered, and concentrated *in vacuo*. The resulting dark-red oil was purified by flash chromatography (CH_2Cl_2, neutral alumina) to yield norbornene-substituted formazan **10** as a dark-red microcrystalline solid that appeared gold in colour under intense lighting. Yield = 1.54 g, 61%. M.p. 110–112 °C. ^{1}H NMR (400.1 MHz, $CDCl_3$): δ 15.35 (br s, 1H, N*H*), δ 8.07 (d, $^3J_{HH}$ = 8 Hz, 2H, aryl C*H*), 7.70 (d, $^3J_{HH}$ = 8 Hz, 4H, aryl C*H*), 7.47 (t, $^3J_{HH}$ = 8 Hz, 4H, aryl C*H*), 7.37 (d, $^3J_{HH}$ = 8 Hz, 2H, aryl C*H*), 7.30 (d, $^3J_{HH}$ = 7 Hz, 2H, aryl C*H*), 6.32–6.28 (m, 1H, =C*H*), 6.22–6.18 (m, 1H, =C*H*), 3.01 (br s, 1H, C*H*), 2.97 (br s, 1H, C*H*), 2.81–2.76 (m, 1H, C*H*), 1.84–1.78 (m, 1H, CH_2), 1.72–1.67 (m, 1H, CH_2), 1.65 (d, $^3J_{HH}$ = 9 Hz, 1H, CH_2), 1.50–1.45 (m, 1H, CH_2). ^{13}C{^{1}H} NMR (150.7 MHz, $CDCl_3$): δ 147.8, 145.6, 141.2, 137.3, 137.2, 134.7, 129.3, 127.6, 127.3, 125.8, 118.7, 48.3, 45.8, 43.5, 42.3, 33.6. FT-IR (KBr): 3,320 (w), 3,057 (m), 2,969 (s), 2,871 (w), 1,598 (s), 1,499 (s), 1,454 (s), 1,355 (m), 1,234 (s) cm^{-1}. UV-Vis (CH_2Cl_2): λ_{max} 491 nm (ε = 9,750 M^{-1} cm^{-1}). Mass Spec. (EI, +ve mode): exact mass calculated for $C_{26}H_{24}N_4$: 392.2001; exact mass found: 392.1994; difference: –1.8 ppm.

Preparation of norbornene-substituted BF_2 formazanate 11

Norbornene-substituted formazan **10** (1.00 g, 2.55 mmol) was dissolved in 150 mL dry toluene. NEt_3 (0.78 g, 1.1 mL, 7.7 mmol) was then added slowly, and the solution was allowed to stir for 10 min. BF_3•OEt_2 (1.8 g, 1.6 mL, 13 mmol) was then added, and the solution was heated to 80 °C and left to stir for 16 h. During this time, the colour of the solution changed from dark red/purple to dark purple. After cooling to room temperature, deionized H_2O (10 mL) was added to quench any excess boron compounds. The toluene solution was then washed with deionized H_2O (3 × 25 mL), dried over $MgSO_4$, gravity filtered, and concentrated *in vacuo*. The resulting dark purple residue was purified by flash chromatography (CH_2Cl_2, neutral alumina) and recrystallized from methanol to yield BF_2 formazante monomer **11** as a dark-purple solid. Yield = 0.60 g, 53%. M.p. 145–147 °C. ^{1}H NMR (399.8 MHz, $CDCl_3$): δ 8.05 (d, $^3J_{HH}$ = 8 Hz, 2H, aryl C*H*), 7.92 (d, $^3J_{HH}$ = 8 Hz, 4H, aryl C*H*), 7.52–7.39 (m, 8H, aryl C*H*), 6.32–6.28 (m, 1H, =C*H*), 6.23–6.19 (m, 1H, =C*H*), 3.02 (br s, 1H, C*H*), 2.97 (br s, 1H, C*H*), 2.83–2.77 (m, 1H, C*H*), 1.84–1.77 (m, 1H, CH_2), 1.74–1.67 (m, 1H, CH_2), 1.63 (d, $^3J_{HH}$ = 9 Hz, 1H, CH_2), 1.50–1.46 (m, 1H, CH_2). ^{13}C{^{1}H} NMR (150.7 MHz, $CDCl_3$): δ 149.4, 147.7, 143.8, 137.4, 137.2, 130.9, 129.6, 129.0, 127.9, 125.4, 123.4, 48.3, 45.8, 43.7, 42.3, 33.7. ^{11}B NMR (128.3 MHz, $CDCl_3$): δ –0.6 (t, $^1J_{BF}$ = 29 Hz). ^{19}F NMR (376.1 MHz, $CDCl_3$): δ –145.1 (q, $^1J_{FB}$ = 29 Hz). FT-IR (KBr): 3,064 (w), 2,961 (m), 2,880 (w), 1,589 (w), 1,490 (m), 1,462 (m), 1,420 (w), 1,356 (m), 1,264 (s) cm^{-1}. UV-Vis (CH_2Cl_2): λ_{max} 518 nm (ε = 15,200 M^{-1} cm^{-1}). Mass Spec. (EI, +ve mode): exact mass calculated for $C_{26}H_{23}BF_2N_4$: 440.1984; exact mass found: 440.2004; difference: +4.5 ppm.

Representative preparation of norbornene-substituted boron difluoride formazanate polymer 12

Norbornene-substituted boron difluoride formazanate monomer **11** (0.10 g, 0.23 mmol) was dissolved in degassed CH_2Cl_2 (9.9 mL), and the solution was left to stir in an ice bath for 15 min. Meanwhile, Grubbs' 3rd generation catalyst (Grubbs III) (0.002 g, 2×10^{-3} mmol, 1 mol %) was dissolved in degassed CH_2Cl_2 (0.1 mL), and the solution was left in an ice bath for 15 min. The catalyst solution was then added to the solution of **11** and the mixture allowed to stir in an ice bath for 5 min. After 5 min, ethyl vinyl ether (0.409 g, 5.68 mmol, 20 equiv.) was added and the solution was allowed to stir for 10 s in an ice bath, and then allowed to reach room temperature while stirring under nitrogen for 30 min. The resulting dark purple polymer was purified by flash chromatography (CH_2Cl_2, neutral alumina) and precipitated from pentane. Norbornene–substituted boron difluoride formazanate polymer **12** was isolated as a purple solid by centrifugation and dried at 40 °C *in vacuo* for 16 h. Yield = 0.090 g, 90%. ^{1}H NMR (399.8 MHz, $CDCl_3$) δ 8.20–7.55 (br m, 7H, aryl C*H*), 7.55–6.80 (br m, 7H, aryl C*H*), 5.23 (br s, 2H, =C*H*), 2.72 (br s, 3H, C*H*), 1.92 (br s, 3H, CH_2), 1.30 (br s, 1 H, CH_2, overlaps with residual pentane CH_2). ^{11}B NMR (128.3 MHz, $CDCl_3$): δ –0.6 (t, $^1J_{BF}$ = 28 Hz), –0.7 (t, $^1J_{BF}$ = 29 Hz). ^{19}F NMR (376.1 MHz, $CDCl_3$): δ –145.1 (br s), –143.2 ppm (br s). FT-IR (KBr): 3,074 (w), 2,998 (w), 2,945 (s), 2,871 (w), 1,589 (s), 1,490 (m), 1,462 (m), 1,431 (w), 1,358 (s), 1,298 (s) cm^{-1}. UV-Vis (CH_2Cl_2): λ_{max} = 518 nm (ε = 14,350 M^{-1} cm^{-1}). GPC (THF, conventional calibration vs. PS standards): M_n = 35,900 g mol^{-1}, M_w = 41,450 g mol^{-1}, $Đ$ = 1.15.

Kinetic studies for the ROMP of BF_2 formazanate monomer 11

Monomer conversion as a function of time

Norbornene-substituted BF_2 formazanate monomer **11** (0.30 g, 0.68 mmol) was dissolved in degassed CH_2Cl_2 (29.6 mL) and the solution was left to stir in an ice bath for 20 min. Meanwhile, Grubbs III (0.006 g, 1 mol%) was dissolved in degassed CH_2Cl_2 (0.4 mL) and left to stir in an ice bath for 20 min. The catalyst solution was then added rapidly in one portion to the solution of **11** and the mixture was allowed to stir in an ice bath. Aliquots of *ca.* 3 mL of this reaction were taken at 1 min intervals (1–8 min), and added to separate flasks containing ethyl vinyl ether (0.1 mL, 2 mmol, *ca.* 25 equiv.) in order to cease polymerization. Each aliquot solution was allowed to reach room temperature while stirring under nitrogen for 30 min. All aliquots were then purified by flash chromatography (CH_2Cl_2 neutral alumina) and analyzed without further purification. The conversion of monomer to polymer was calculated based on the comparison between the integration values determined by ^{1}H NMR spectroscopy for the vinyl groups of monomer **11** (m, 6.32–6.28 ppm and m, 6.23–6.19 ppm) and polymer **12** (br s, 5.23 ppm). A semilogarithmic plot was constructed based on the calculated degree of monomer conversions at different times.

Molecular weight as a function of catalyst:monomer ratio

In five separate flasks, monomer **11** (0.030 g, 0.068 mmol) was dissolved in degassed CH_2Cl_2 to yield a final reaction concentration of 10 mg mL^{-1}; these solutions were left to stir in an ice bath for 20 min. Meanwhile, Grubbs III (0.015 g, 0.17 mmol) was dissolved in degassed CH_2Cl_2 (2 mL) and left to stir in an ice bath for 20 min. Various amounts of the catalyst solution were then added to each solution of **11** in order to yield the following catalyst:monomer ratios: 1:100, 1:80, 1:60, 1:40, 1:20. After 5 min, ethyl vinyl ether (0.1 mL, 2 mmol, *ca.* 25 equiv.) was added to cease polymerization, and the individual reactions were allowed to reach room temperature while stirring under nitrogen for 30 min. The resulting polymers were then purified by flash chromatography (CH_2Cl_2 neutral alumina) and analyzed without further purification. The degree of polymerization for each polymer studied was determined by GPC analysis in THF (conventional calibration vs. polystyrene).

Results and discussion

Monomer Synthesis and Characterization

The synthetic approach employed for monomer synthesis are shown in Scheme 1. Briefly, 4-(bicyclo[2.2.1]hept-5-en-2-yl)benzaldehyde **8** was combined with phenylhydrazine to form hydrazone **9**, which was isolated by filtration and used without further purification (Fig. S2). Hydrazone **9** was converted to norbornene-substituted formazan **10** under biphasic conditions, following the procedure originally developed by Katritzky and co-workers.[17] It should be noted that hydrazone **9** and phenyldiazonium chloride must be added to the biphasic mixture in quick succession as prolonged stirring of hydrazone **9** in this mixture resulted in decomposition. The formation of formazan **10** was confirmed using ^{1}H NMR spectroscopy (NH at 15.35 ppm) and UV-Vis absorption spectroscopy (λ_{max} = 491 nm, ε = 9,750 M^{-1} cm^{-1}), which were consistent with other triarylformazans (Figs. S3, S4).[5d] Formazan **10** was transformed into its corresponding BF_2 complex **11** by heating it in the presence of excess BF_3•OEt_2 and NEt_3 in toluene. This transformation was accompanied by a loss of the formazan NH resonance in the ^{1}H NMR spectrum and the appearance of a triplet (–0.6 ppm, $^1J_{BF}$ = 29 Hz) and quartet (–145.1 ppm, $^1J_{FB}$ = 29 Hz) in the ^{11}B and ^{19}F NMR spectra collected for BF_2 monomer **11** (Figs. S5–S8). The relatively low isolated yield of 53% for monomer **11** reflects our emphasis on purity, which was a priority given our desire to explore its subsequent polymerization reactivity. For many application, purification by column chromatography alone may be sufficient.

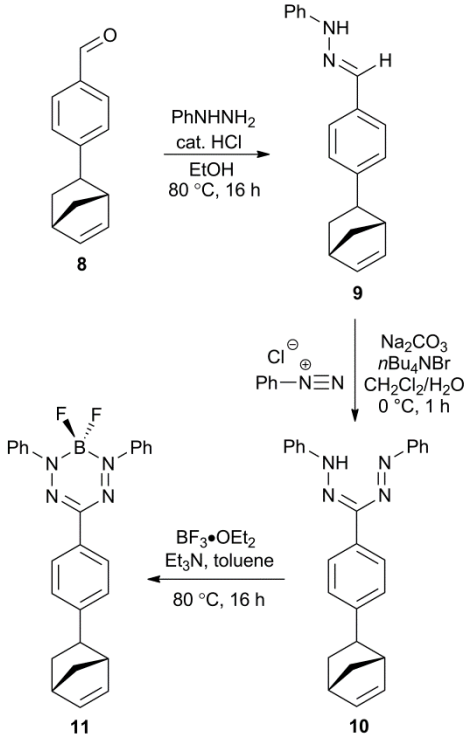

Scheme 1 Synthetic pathway for the realization of BF_2 formazanate monomer **11**.

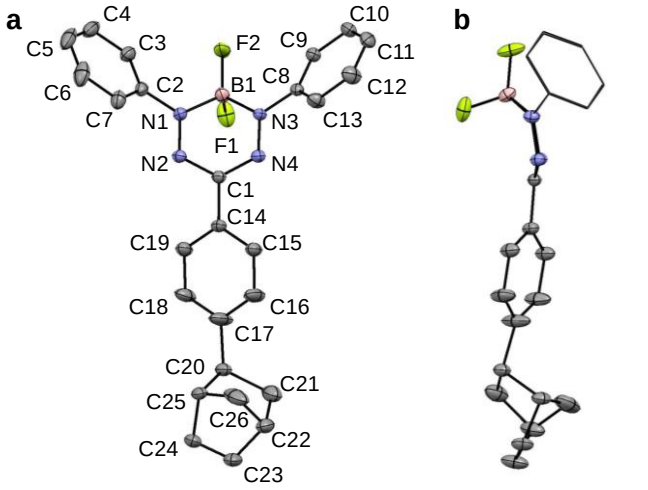

Fig. 1 Top (a) and side (b) views of the solid-state structure of BF_2 formazanate monomer **11**. Selected bond lengths (Å): N1-N2 1.316(2), N3-N4 1.307(2), C1-N2 1.341(2), C1-N4 1.350(2), N1-B1 1.553(3), N3-B1 1.560(2), C20-C21 1.623(4), C23-C24 1.333(3). Selected bond angles (deg.): N1-N2-C1 116.3(1), N3-N4-C1 116.8(1), N1-B1-N3 100.9(1), N2-C1-N4 124.1(1).

Single crystals of monomer **11** (monoclinic, P 2_1/n) were grown by diffusion of hexanes into a saturated solution in CH_2Cl_2 (Fig. 1, Table 1). The norbornene unit was disordered and two distinct occupancies at an angle of 77° to one another were resolved. The solid-state structure of **11** shares many structural features in common with other BF_2 triarylformazanate complexes.[5b, 5d, 5f] The N-N (N1-N2 1.316(2) Å, N3-N4 1.307(2) Å) and C-N (C1-N2 1.341(2) Å, C1-N4 1.350(2) Å) bond lengths of the formazanate ligand are essentially symmetric and in between the typical bond lengths of single and double bonds of the respective atoms.[18] The *N*-aryl substituents are twisted by 52.9 and 49.5° relative to the N_4 plane, in what has been previously coined as a 'dragonfly' conformation.[5c] The B1 and C1 atoms are displaced from the N_4 plane by 0.64 and 0.22 Å, which exists at a torsion angle of 30.5° with respect to the *p*-substituted phenyl spacer (C14–C19). Based on the solid-state structure and related NMR spectra that are consistent with the presence of a single compound (Figs. S5–S8), we concluded that complex **11** exists exclusively as the *exo*-isomer.

Polymer Synthesis and Characterization

Based on the exceptional functional group tolerance and molecular weight control generally associated with ROMP,[19] we chose to explore its suitability for the preparation of BF_2 formazanate polymers. Our polymerization reactions were carried out at monomer concentrations of *ca.* 10 mg mL^{-1} in dry and degassed CH_2Cl_2 at 0 °C using Grubbs III (3-bromo-pyridine derivative) and ethyl vinyl ether as a capping/terminating agent according to Scheme 2.[20]

In order to further probe the suitability of ROMP for the polymerization of monomer **11**, we conducted two different kinetic studies. The scope of our studies was limited by the fact that the ^{1}H NMR resonances associated with the phenyl end group overlapped with those of the phenyl groups of the polymer repeating unit. Furthermore, the polymers described were found to absorb the 630 nm wavelength laser that we typically employ during light-scattering experiments. Nonetheless, we set out to monitor a ROMP reaction between monomer **11** and Grubbs III over a period of 8 min in order to construct a semi-logarithmic plot (Fig. 2). The linear nature of the plot, which was constructed using the ratios of the ^{1}H NMR integrations of the vinyl protons in the monomer (m, 6.32–6.28 ppm and m, 6.23–6.19 ppm) and polymer (br s, 5.23

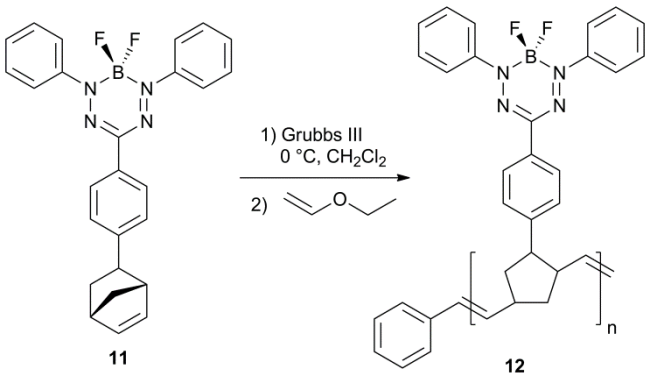

Scheme 2 Generic reaction scheme for the ROMP of BF_2 formazanate monomer **11** to afford polymer **12**.

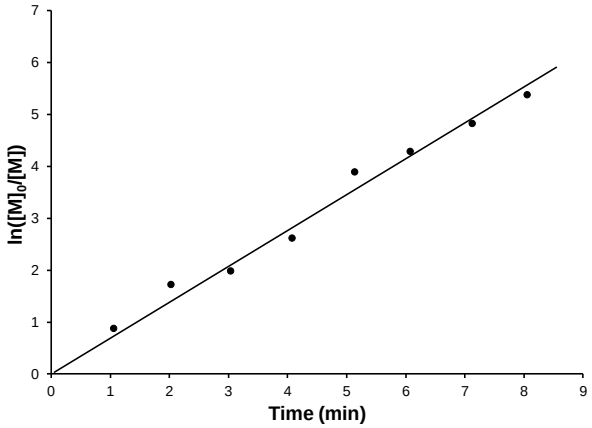

Fig. 2 Semilogarithmic plot for the consumption of BF_2 formazanate monomer **11** as a function of time. The black line is a best fit trendline for the data.

ppm), confirmed that monomer consumption was consistent with living ROMP.

We conducted a second study designed to probe the relationship between feed molar ratio and the number average degree of polymerization (DP_n), determined by conventional calibration GPC analysis (Fig. 3a, M_n 9,250–69,000 g mol^{-1}, $Đ$ 1.12–1.29). Despite previous indications that the ROMP of monomer **11** may occur in a living fashion, we observed a deviation from ideal polymerization behaviour during this second study. When high molecular weight polymers were targeted (lower catalyst:monomer ratios), lower than expected values of DP_n were observed. Furthermore, as the catalyst:monomer ratio was decreased, a high molecular weight shoulder began to appear in the corresponding GPC traces (Fig. 3b). Considering that the consumption of monomer **11** was consistent with a living ROMP, we postulate that, under the conditions employed, chain propagation competes with chain coupling reactions. The proposed chain coupling reactions would account for the larger high molecular weight shoulders observed as higher molecular weights were targeted. In order to probe this behaviour further, we stirred a purified sample of polymer **12** with Grubbs III under the same conditions employed for polymerization. Aliquots of the reaction mixture were removed after 5, 15, and 30 min, terminated with ethyl vinyl ether, and passed through a neutral alumina column (CH_2Cl_2) to remove the catalyst. GPC analysis revealed no change in the molecular weight distribution for each aliquot (Fig. S9), indicating that Grubbs III does not readily react with the unstrained alkenes present in the polymer backbone. Thus, we conclude that chain coupling must involve the propagating chain end exclusively. Furthermore, based on the monomer consumption studies discussed previously, we postulate that chain coupling does not result in catalyst poisoning. Similar chain coupling reactions were not reported when Grubbs III was employed for the polymerization of related redox-active monomers based on nitronyl nitroxide radicals[10] and cobaltocenium moieties.[21]

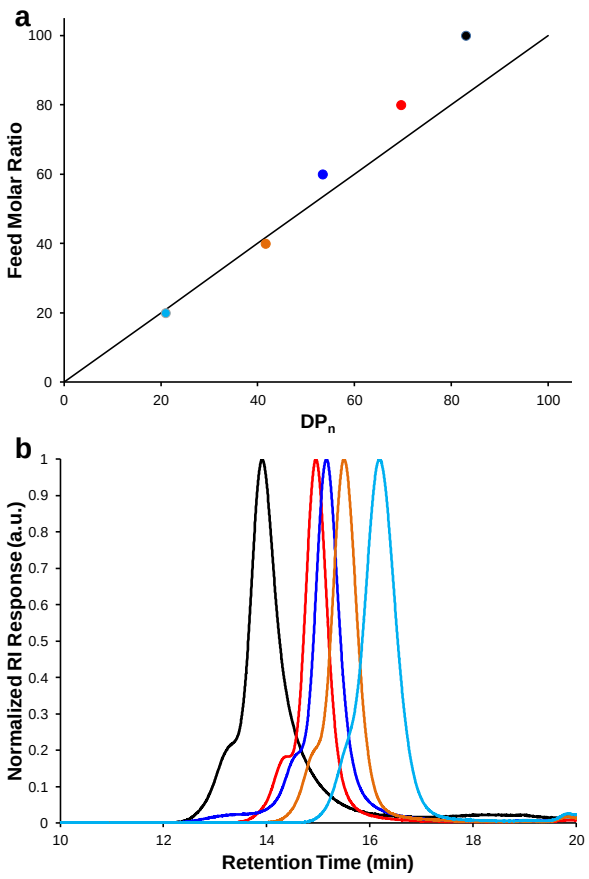

Fig. 3 Relationship between the DP_n of BF_2 formazanate polymer **12** determined by GPC analysis and the molar feedstock ratio (a) and corresponding GPC traces (b). The black line represents the theoretical relationship between feed molar ratio and DP_n.

Based on our kinetic studies, we prepared a sample of polymer **12** for comparison with monomer **11**, stopping the polymerization reaction before complete conversion in order to minimize the degree of chain coupling and/or side reactivity (90% isolated yield; GPC: M_n = 35,900 g mol^{-1}, M_w = 41,450 g mol^{-1}, $Đ$ = 1.15). The ^{1}H NMR spectrum of polymer **12** was broadened compared to that of monomer **11**, and was comprised of resonances corresponding to the proposed structure (Fig. S10). The ^{11}B and ^{19}F NMR spectra of polymer **12** each contained two resonances that we believe correspond to head-to-tail (major) and head-to-head and/or tail-to-tail (minor) diads within the polymer backbone (Figs. S11, S12). Upon heating, polymer **12** degraded gradually up to a temperature of 237 °C, at which time it had lost 3% of its mass. Above 237 °C, the polymer degraded in two steps corresponding to 32% and 40% mass loss, respectively. At 775 °C, 28% of the initial mass remained (Fig. S13). The glass transition temperature (T_g) determined for polymer **12** was 161 °C (Fig. S14).

UV-Vis Absorption and Emission Spectroscopy

The UV-Vis absorption and emission spectra collected for monomer **11** and polymer **12** in CH_2Cl_2 are quite similar (Fig. 4, S15, and S16). The lowest energy absorptions for both complexes occur at λ_{max} = 518 nm (ε ~ 14,750 M^{-1} cm^{-1}) and are red-shifted by 27 nm when compared to formazan **10**. The highest occupied molecular orbital (HOMO) and lowest unoccupied molecular orbital (LUMO) have previously been shown as the dominant orbital pair ($\pi \rightarrow \pi^*$) involved in the lowest energy excitation computed for similar compounds using time-dependent density functional theory (TDDFT).[5e] The close agreement of the spectra confirms that the pendant BF_2 formazanate groups of polymer **12** tolerate the ROMP reaction, and also that through space electron transfer does not occur readily along the polymer backbone. The thin-film absorption spectrum of polymer **12** was red-shifted, but qualitatively very similar to the solution-based spectrum (Fig. 4b), further confirming that the side-chain BF_2 formazanate groups are electronically isolated in the polymer. Both monomer and polymer are weakly emissive in solution, with wavelengths of maximum emission (λ_{em}) of 645 nm and quantum yields (Φ_F) of 1.5% for **11** and 2.5% for **12**.[22] The large Stoke's shifts (υ_{ST}) of 127 nm (3,800 cm^{-1}) are consistent with other BF_2 complexes of triarylformazanates,[5d] and we are actively exploring the origin of this phenomena in our laboratory. Compared to similar side-chain BODIPY polymers [*e.g.*, 4: λ_{max} = 520 nm, λ_{em} = 540 nm, Φ_F = 0.37, υ_{ST} = 20 nm (712 cm^{-1})],[3d] the absorption and emission maxima of polymer **12** were red-shifted, the observed fluorescence intensity (quantum yield) was significantly lower, and the Stoke's shift was significantly larger.

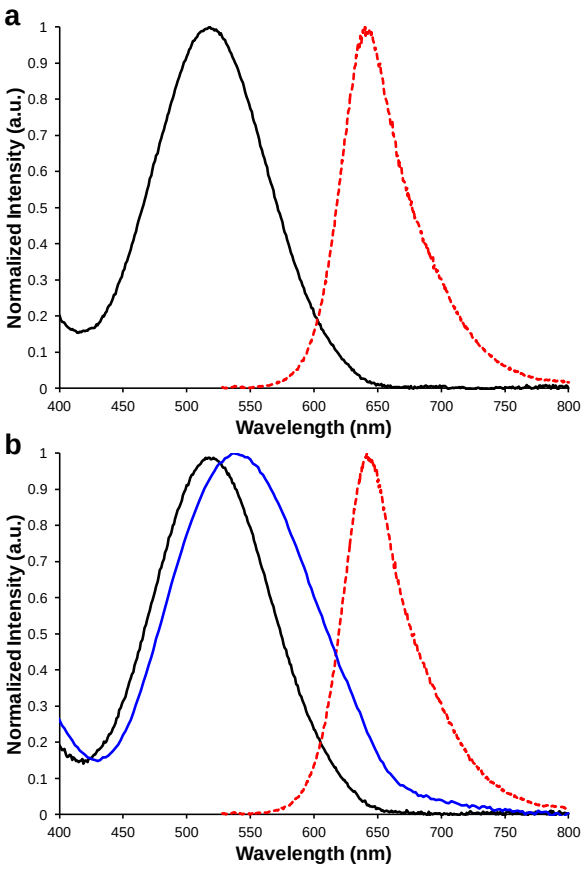

Fig. 4 Solution phase UV-Vis absorption (black lines) and emission (red, dashed lines) spectra recorded in CH_2Cl_2 and thin-film UV-Vis absorption spectrum (blue line) of BF_2 formazanate monomer **11** (a) and polymer **12** (b).

Cyclic Voltammetry

The electrochemical properties of BF_2 formazanate monomer **11** and polymer **12** were examined by conducting cyclic voltammetry (CV) studies in CH_2Cl_2 and THF (Figs. 5, S17, and S18). Upon scanning to negative potentials, monomer **11** undergoes two one-electron reductions to form its ligand-centred radical anion (E°_{red1} = –0.97 mV; $LBF_2 \leftrightarrows LBF_2^{\bullet-}$, L = formazanate ligand) and dianion (E°_{red2} = –1.92 V; $LBF_2^{\bullet-} \rightarrow LBF_2^{2-}$) forms. The second reduction is not formally reversible, indicating that the extremely electron-rich dianion formed undergoes a chemical reaction on the timescale of the CV experiment. Crucially, based on the fact that the first reduction wave is reversible, this chemical reaction must regenerate the radical anion form of monomer **11**, which is subsequently oxidized to form the neutral form of monomer **11**. The observed behaviour is consistent with previous reports for similar compounds,[5f] but differs from the reactivity pathways previously described by Otten and co-workers, whereby a number of unique products were observed upon chemical reduction with Na/Hg amalgum.[5g] The CV of polymer **12** illustrates significantly different behaviour. The first reduction wave (E°_{red1} = –0.95 V) is broadened compared to what was observed for monomer **11**, and the current response was significantly lower than expected. Both observations are consistent with a lack of diffusion control at the working electrode, a common problem encountered when analyzing macromolecules. Of particular significance is the absence of a second reduction wave for the polymer. Upon conversion of the neutral form of polymer **12** to its poly(radical anion) form, we believe that each repeating unit of the polymer exists in an

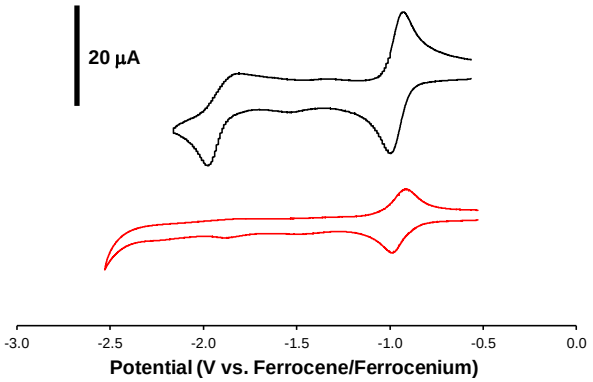

Fig. 5 Cyclic voltammograms for BF_2 formazanate monomer **11** (black line) and polymer **12** (red line) recorded in dry, degassed CH_2Cl_2 containing ~ 1 mM analyte and 0.1 M nBu_4NPF_6 at a scan rate of 250 mV s^{-1}.

extremely electron-rich environment due to the close proximity of neighbouring anions along the polymer backbone. We assume that the second reduction would occur outside of the electrochemical window for CH_2Cl_2 and THF, and is therefore not observed. The reversibility of the first reduction wave supports our argument and disfavours alternative explanations involving decomposition of the poly(radical anion) form of the polymer.

Conclusions

We have thoroughly investigated the ROMP of a novel norbornene-containing BF_2 formazanate monomer. During the polymerization, which readily occurs in the presence of BF_2 formazantes, monomer **11** is consumed in a fashion consistent with a living polymerization. However, studies involving variation of the feed molar ratio revealed a loss of control when higher molecular weights were targeted, indicating that chain coupling and/or side reactions compete with chain propagation. The absorption/emission properties of the resulting polymer **12**, which can be prepared with reasonable molecular weight control, were in close agreement with those of the monomer. CV studies revealed significantly different behaviour, whereby the expected reduction of the polymer from the poly(radical anion) form to the poly(dianion) form was not observed, presumably due to the extremely electron-rich environment created upon the initial reduction of the polymer. Our future work in this area will involve expansion of the methodologies described to include a wide range of BF_2 formazanate polymers and exploration of their redox and light harvesting properties.

Acknowledgements

We would like to thank the University of Western Ontario, the Natural Science and Engineering Research Council (NSERC) of Canada (J.B.G.: DG, 435675 and S.N., J.A.P., S.M.B., R.R.M.: postgraduate scholarships), and the Ontario Ministry of Research and Innovation (J.B.G.: ERA, ER14-10-147) for funding this work. Finally, we thank Dr. Elizabeth R. Gillies and Dr. Paul J. Ragogna for access to instrumentation in their laboratories.

Notes and references

1 Review: X. He and T. Baumgartner, *RSC Adv.*, 2013, **3**, 11334–11350.

2 Selected examples: (a) A. Lorbach, M. Bolte, H. Li, H.-W. Lerner, M. C. Holthausen, F. Jäkle and M. Wagner, *Angew. Chem. Int. Ed.*, 2009, **48**, 4584–4588; (b) B. Kim, B. Ma, V. R. Donuru, H. Liu and J. M. J. Fréchet, *Chem. Commun.*, 2010, **46**, 4148–4150; (c) D. R. Levine, M. A. Siegler and J. D. Tovar, *J. Am. Chem. Soc.*, 2014, **136**, 7132–7139; (d) S. Zhang, Y. Sheng, G. Wei, Y. Quan, Y. Cheng and C. Zhu, *J. Polym. Sci., Part A: Polym. Chem.*, 2014, **52**, 1686–1692; (e) R. Yoshii, A. Hirose, K. Tanaka and Y. Chujo, *J. Am. Chem. Soc.*, 2014, **136**, 18131–18139; (f) R. Yoshii, H. Yamane, K. Tanaka and Y. Chujo, *Macromolecules*, 2014, **47**, 3755-3760; (g) I. A. Adams and P. A. Rupar, *Macromol. Rapid Commun.*, 2015, **36**, 1336–1340; (h) C. Dai, D. Yang, X. Fu, Q. Chen, C. Zhu, Y. Cheng and L. Wang, *Polym. Chem.*, 2015, **6**, 5070–5076; (i) C.-T. Poon, D. Wu, W. H. Lam and V. W.-W. Yam, *Angew. Chem. Int. Ed.*, 2015, **54**, 10569–10573; (j) V. M. Suresh, A. Bandyopadhyay, S. Roy, S. K. Pati and T. K. Maji, *Chem. Eur. J.*, 2015, **21**, 10799–10804.

3 Selected examples: (a) R. Stahl, C. Lambert, C. Kaiser, R. Wortmann and R. Jakober, *Chem. Eur. J.*, 2006, **12**, 2358–2370; (b) C.-H. Zhao, A. Wakamiya and S. Yamaguchi, *Macromolecules*, 2007, **40**, 3898–3900; (c) D. Reitzenstein and C. Lambert, *Macromolecules*, 2009, **42**, 773–782; (d) A. Nagai, K. Kokado, J. Miyake and Y. Chujo, *Macromolecules*, 2009, **42**, 5446–5452; (e) Y. Hu, Z. Zhao, X. Bai, X. Yuan, X. Zhang and T. Masuda, *RSC Adv.*, 2014, **4**, 55179–55186; (f) F. Guo, X. Yin, F. Pammer, F. Cheng, D. Fernandez, R. A. Lalancette and F. Jäkle, *Macromolecules*, 2014, **47**, 7831–7841; (g) B. Liu, L. Li, C. Lin, J. Zhou, Z. Zhu, H. Xu, H. Qiu and S. Yin, *Polym. Chem.*, 2014, **5**, 372–381; (h) H. Yeo, K. Tanaka and Y. Chujo, *J. Polym. Sci., Part A: Polym. Chem.*, 2015, **53**, 2026–2035.

4 Reviews: (a) C. D. Entwistle and T. B. Marder, *Chem. Mater.*, 2004, **16**, 4574–4585; (b) N. Matsumi and Y. Chujo, *Polym. J.*, 2008, **40**, 77–89; (c) F. Jäkle, *Chem. Rev.*, 2010, **110**, 3985–4022.

5 Selected examples: (a) J. B. Gilroy, M. J. Ferguson, R. McDonald, B. O. Patrick and R. G. Hicks, *Chem. Commun.*, 2007, 126–128; (b) M.-C. Chang and E. Otten, *Chem. Commun.*, 2014, **50**, 7431–7433; (c) S. M. Barbon, P. A. Reinkeluers, J. T. Price, V. N. Staroverov and J. B. Gilroy, *Chem. Eur. J.*, 2014, **20**, 11340–11344; (d) S. M. Barbon, J. T. Price, P. A. Reinkeluers and J. B. Gilroy, *Inorg. Chem.*, 2014, **53**, 10585–10593; (e) S. M. Barbon, V. N. Staroverov and J. B. Gilroy, *J. Org. Chem.*, 2015, **80**, 5226–5235; (f) S. M. Barbon, J. T. Price, U. Yogarajah and J. B. Gilroy, *RSC Adv.*, 2015, **5**, 56316–56324; (g) M.-C. Chang and E. Otten, *Inorg. Chem.*, 2015, **54**, 8656–8664; (h) R. R. Maar, S. M. Barbon, N. Sharma, H. Groom, L. G. Luyt and J. B. Gilroy, *Chem. Eur. J.*, 2015, **21**, 15589–15599.

6 Selected examples: (a) D. A. Brown, H. Bögge, G. N. Lipunova, A. Müller, W. Plass and K. G. Walsh, *Inorg. Chim. Acta*, 1998, **280**, 30–38; (b) J. B. Gilroy, B. O. Patrick, R. McDonald and R. G. Hicks, *Inorg. Chem.*, 2008, **47**, 1287–1294; (c) S. Hong, L. M. R. Hill, A. K. Gupta, B. D. Naab, J. B. Gilroy, R. G. Hicks, C. J. Cramer and W. B. Tolman, *Inorg. Chem.*, 2009, **48**, 4514–4523; (d) M.-C. Chang, T. Dann, D. P. Day, M. Lutz, G. G. Wildgoose and E. Otten, *Angew. Chem. Int. Ed.*, 2014, **53**, 4118–4122; (e) R. Travieso-Puente, M.-C. Chang and E. Otten, *Dalton Trans.*, 2014, **43**, 18035–18041; (f) M.-C. Chang, P. Roewen, R. Travieso-Puente, M. Lutz and E. Otten, *Inorg. Chem.*, 2015, **54**, 379–388; (g) N. A. Protasenko, A. I. Poddel'sky, A. S. Bogomyakov, G. K. Fukin and V. K. Cherkasov, *Inorg. Chem.*, 2015, **54**, 6078–6080.

7 Reviews: (a) A. W. Nineham, *Chem. Rev.*, 1955, **55**, 355–483; (b) A. S. Shawali and N. A. Samy, *J. Adv. Res.*, 2015, **6**, 241–254.

8 Review: L. Bourget-Merle, M. F. Lappert and J. R. Severn, *Chem. Rev.*, 2002, **102**, 3031–3066.

9 M. Hesari, S. M. Barbon, V. N. Staroverov, Z. Ding and J. B. Gilroy, *Chem. Commun.*, 2015, **51**, 3766–3769.

10 T. Sukegawa, A. Kai, K. Oyaizu and H. Nishide, *Macromolecules*, 2013, **46**, 1361–1367.

11 K. Suzuki, A. Kobayashi, S. Kaneko, K. Takehira, T. Yoshihara, H. Ishida, Y. Shiina, S. Oishi and S. Tobita, *Phys. Chem. Chem. Phys.*, 2009, **11**, 9850–9860.

12 S. Fery-Forgues and D. Lavabre, *J. Chem. Educ.*, 1999, **76**, 1260–1264.

13 Bruker-AXS, SAINT version 2013.8, 2013, Bruker-AXS, Madison, WI 53711, USA.

14 Bruker-AXS, SADABS version 2012.1, 2012, Bruker-AXS, Madison, WI 53711, USA.

15 G. M. Sheldrick, *Acta Crystallogr.*, 2015, **A71**, 3–8.

16 G. M. Sheldrick, *Acta Crystallogr.*, 2008, **A64**, 112–122.

17 A. A. Katritzky, S. A. Belyakov, D. Cheng and H. D. Durst, *Synthesis*, 1995, **1995**, 577–581.

18 W. M. Haynes, *CRC Handbook of Chemistry and Physics*, CRC Press, Boca Raton, Fla, 2012.

19 Reviews: (a) C. W. Bielawski and R. H. Grubbs, *Prog. Polym. Sci.*, 2007, **32**, 1–29; (b) F. Blank and C. Janiak, *Coord. Chem. Rev.*, 2009, **253**, 827–861; (c) S. Sutthasupa, M. Shiotsuki and F. Sanda, *Polym. J.*, 2010, **42**, 905–915.

20 At monomer concentrations exceeding 10 mg mL^{-1}, polymerization reactions went to completion in 1–2 min and broadened molecular weight distributions were observed.

21 L. Ren, J. Zhang, X. Bai, C. G. Hardy, K. D. Shimizu and C. Tang, *Chem. Sci.*, 2012, **3**, 580–583.

22 Thin films of polymer **12** were non-emissive under long-wave UV irradiation (365 nm).

Supplementary Information

Side-Chain Boron Difluoride Formazanate Polymers via Ring-Opening Metathesis Polymerization

*Samantha Novoa, Joseph A. Paquette, Stephanie M. Barbon, Ryan R. Maar and Joe B. Gilroy**

Department of Chemistry and the Centre for Advanced Materials and Biomaterials Research (CAMBR), The University of Western Ontario, 1151 Richmond St. N., London, Ontario, Canada, N6A 5B7. Tel: +1-519-661-2111 ext. 81561, E-mail: joe.gilroy@uwo.ca.

Emission Correction Data

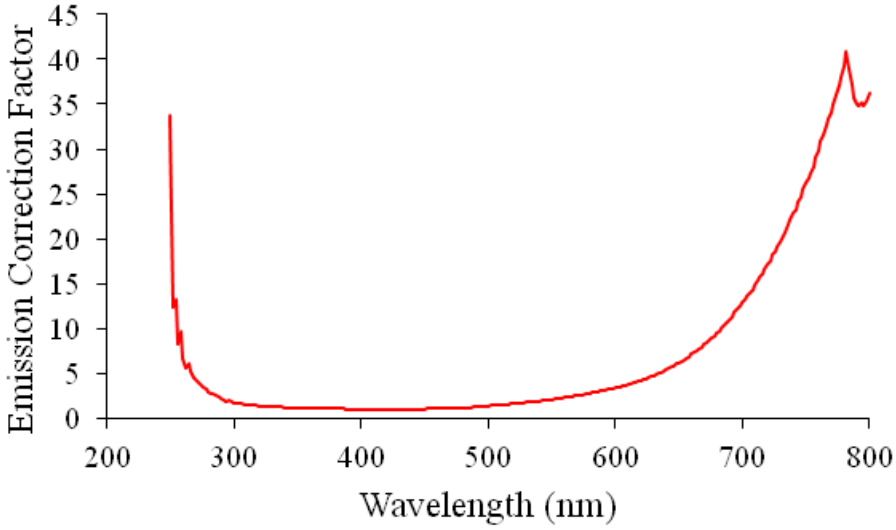

Fig. S1 Wavelength-dependent emission correction provided by Photon Technology International.

NMR Spectra

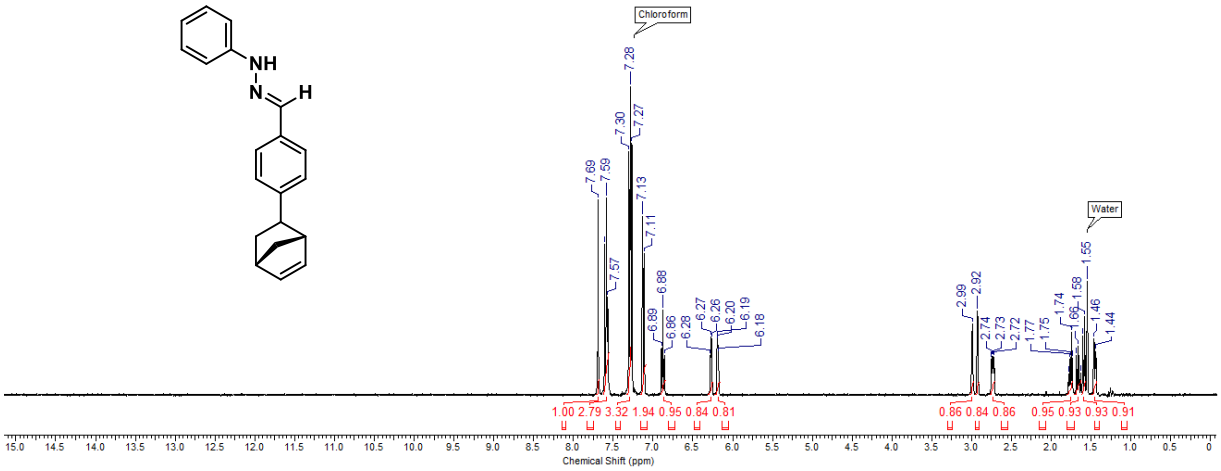

Fig. S2 ^{1}H NMR spectrum of hydrazone **9** in $CDCl_3$.

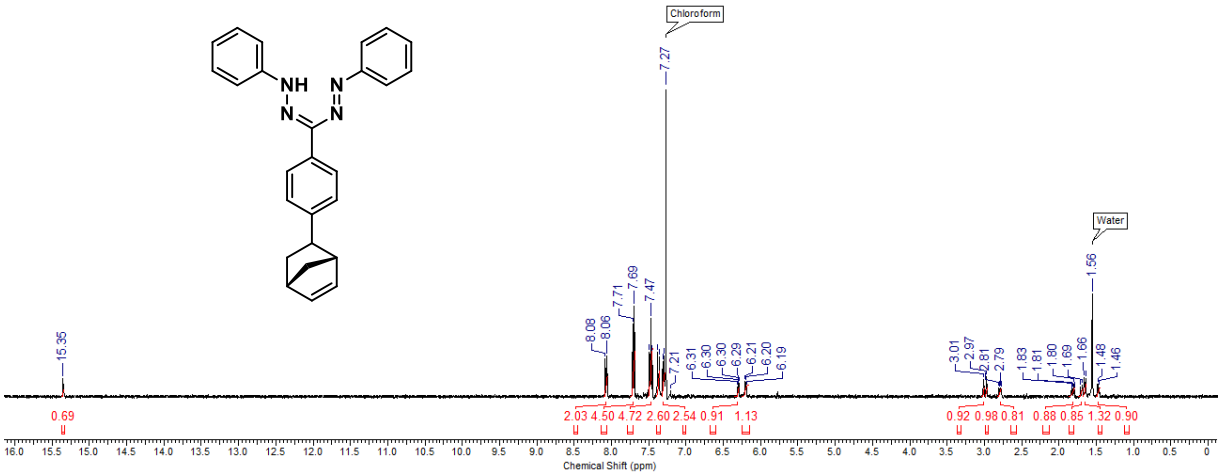

Fig. S3 ^{1}H NMR spectrum of formazan **10** in $CDCl_3$.

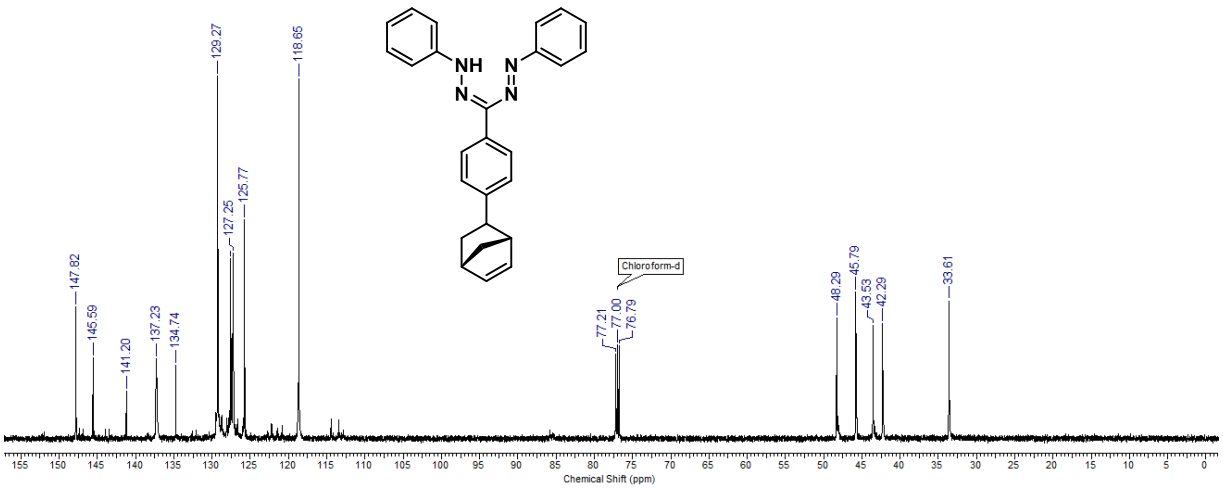

Fig. S4 $^{13}C\{^{1}H\}$ NMR spectrum of formazan **10** in $CDCl_3$.

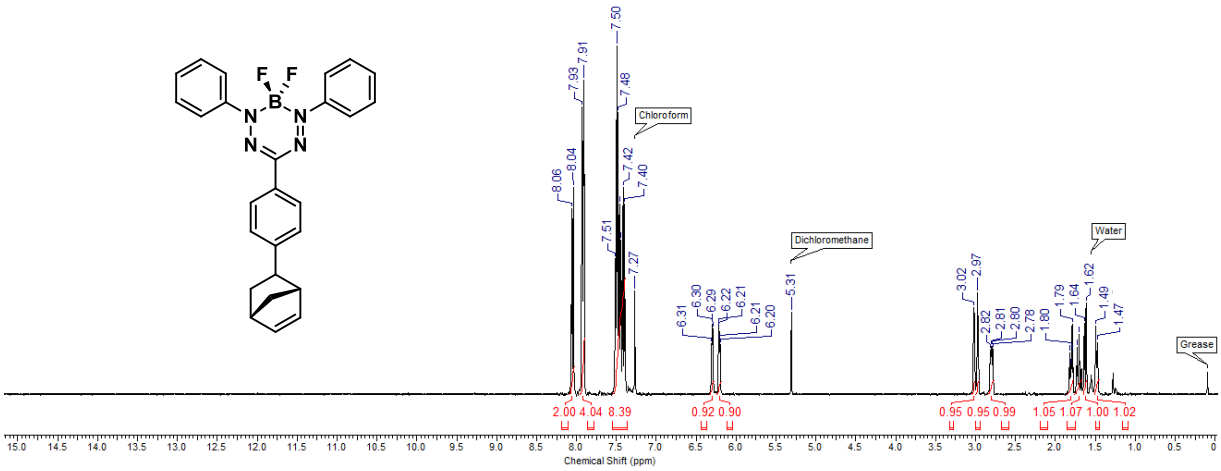

Fig. S5 ^{1}H NMR spectrum of BF_2 formazanate monomer **11** in $CDCl_3$.

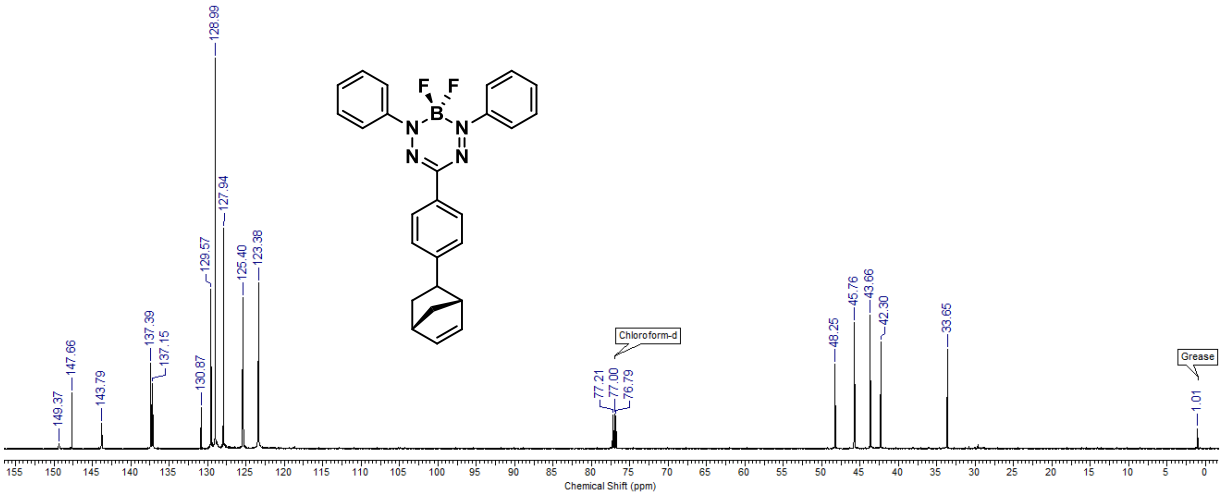

Fig. S6 $^{13}C\{^{1}H\}$ NMR spectrum of BF_2 formazanate monomer **11** in $CDCl_3$.

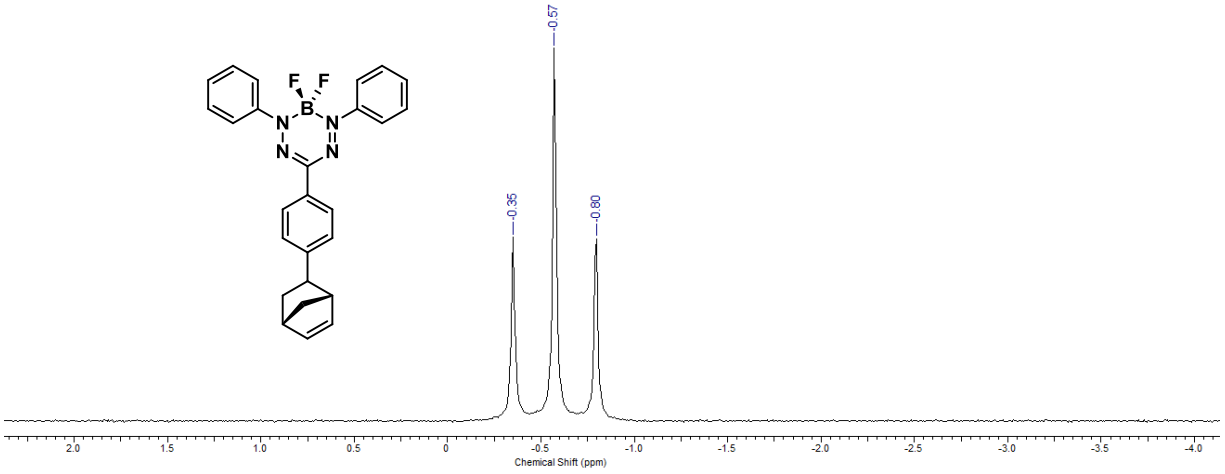

Fig. S7 ^{11}B NMR spectrum of BF_2 formazanate monomer **11** in $CDCl_3$.

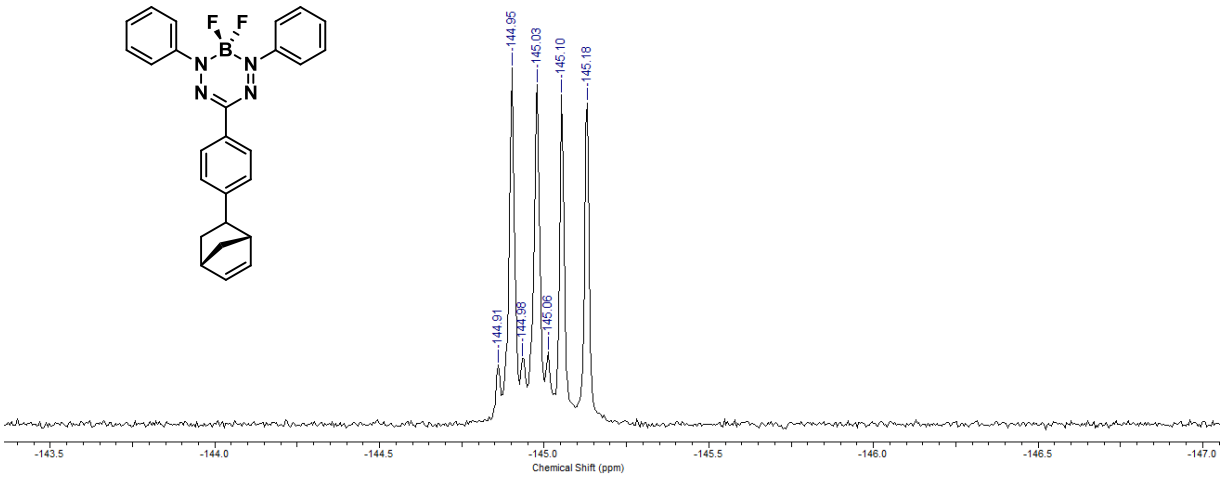

Fig. S8 ^{19}F NMR spectrum of BF_2 formazanate monomer **11** in $CDCl_3$.

Additional GPC Data

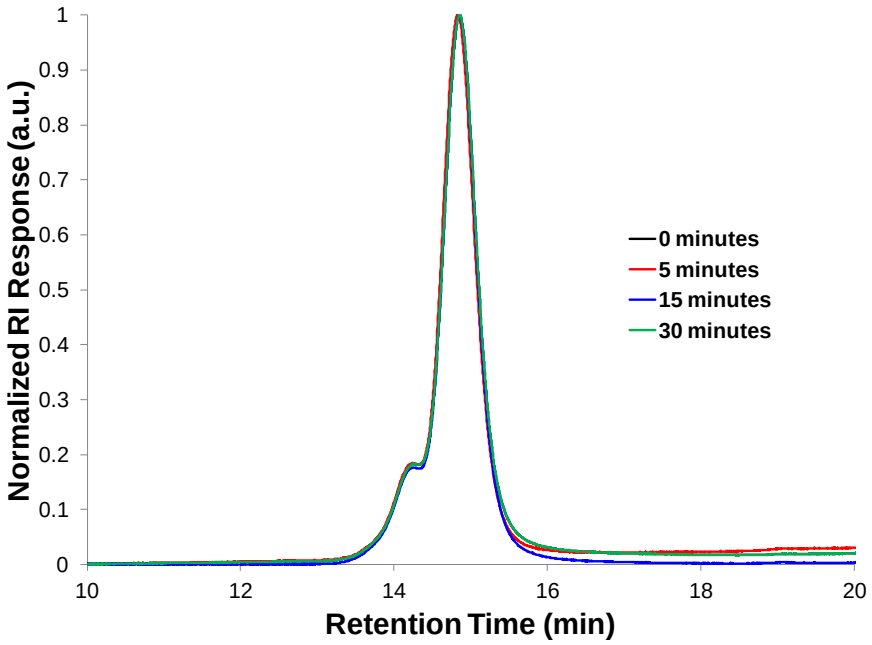

Fig. S9 GPC Traces for Control Experiment Involving the Reaction of Grubbs' 3rd Generation Catalyst with Polymer 12.

Polymer NMR Data

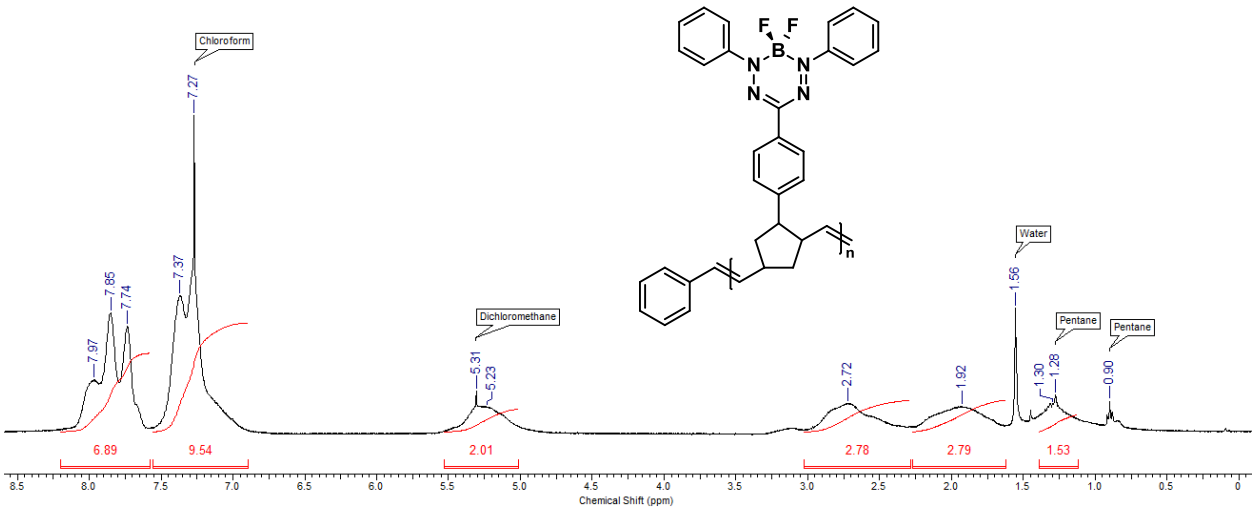

Fig. S10 ^{1}H NMR spectrum of BF_2 formazanate polymer **12** in $CDCl_3$.

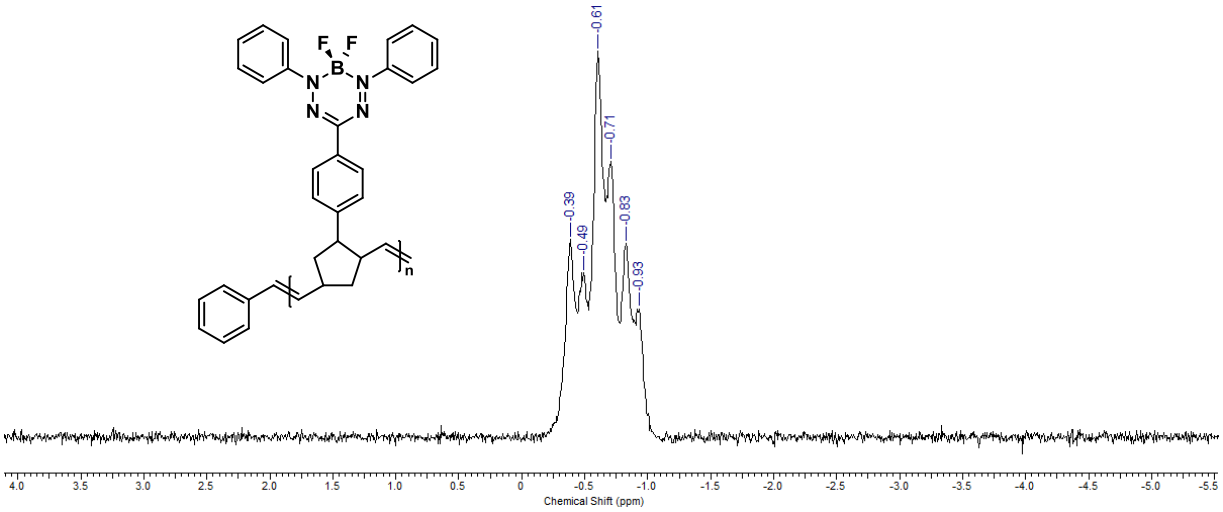

Fig. S11 ^{11}B NMR spectrum of BF_2 formazanate polymer **12** in $CDCl_3$.

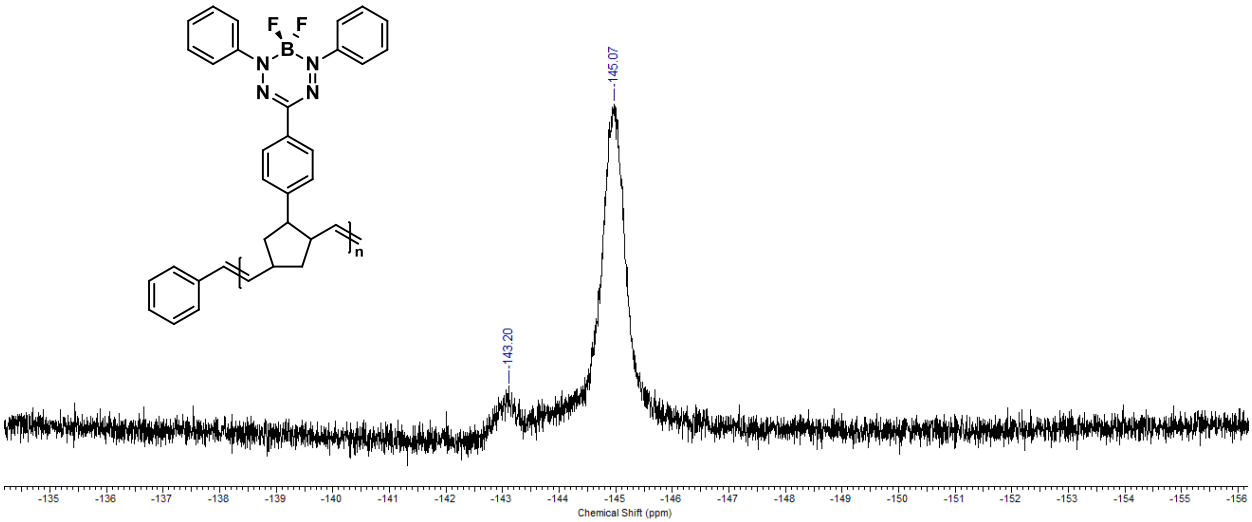

Fig. S12 ^{19}F NMR spectrum of BF_2 formazanate polymer **12** in $CDCl_3$.

Thermal Analysis

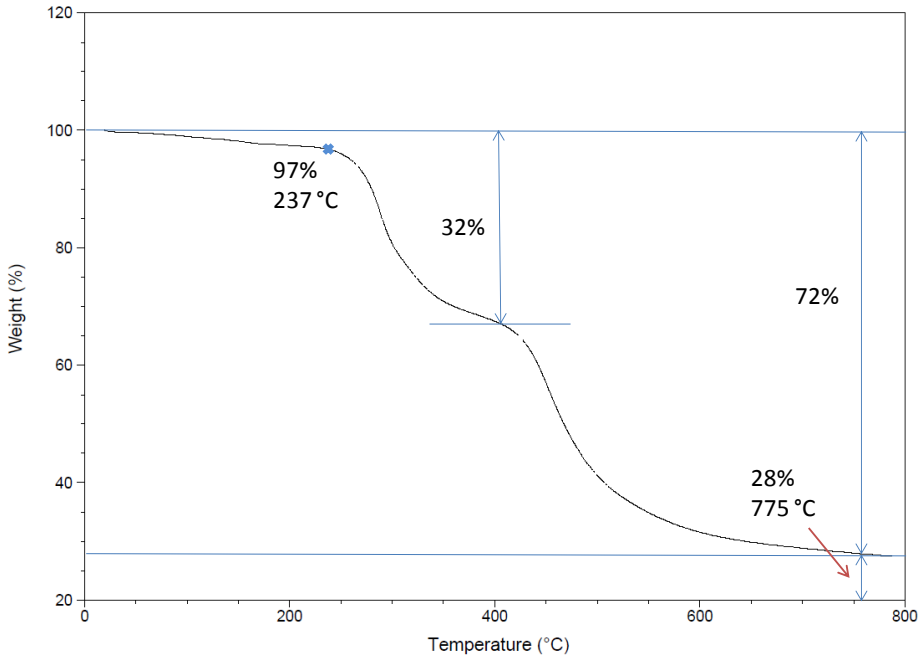

Fig. S13 TGA trace for BF_2 formazanate polymer **12**.

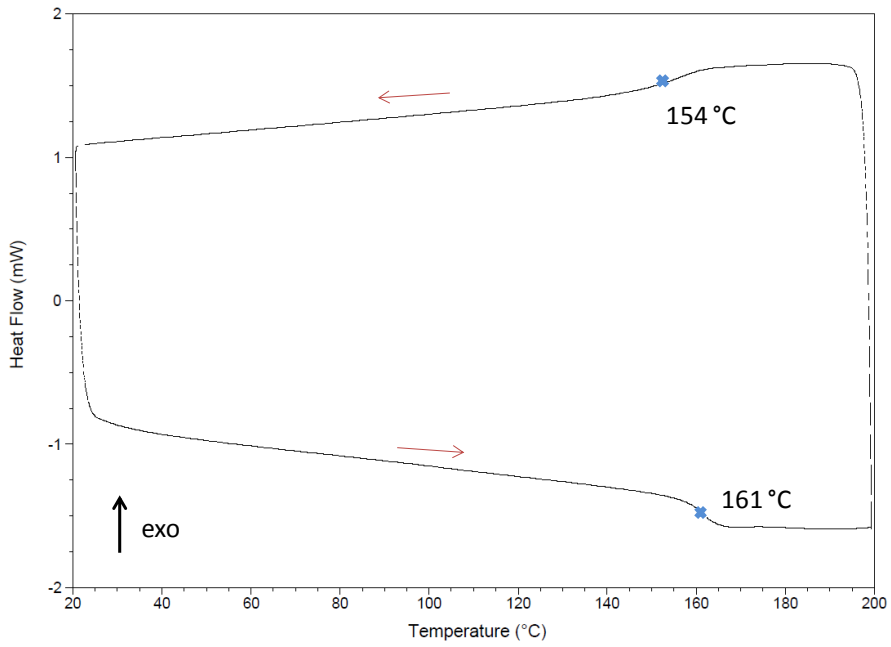

Fig. S14 DSC thermogram collected for BF_2 formazanate polymer **12**.

UV-Vis Absorption Spectra

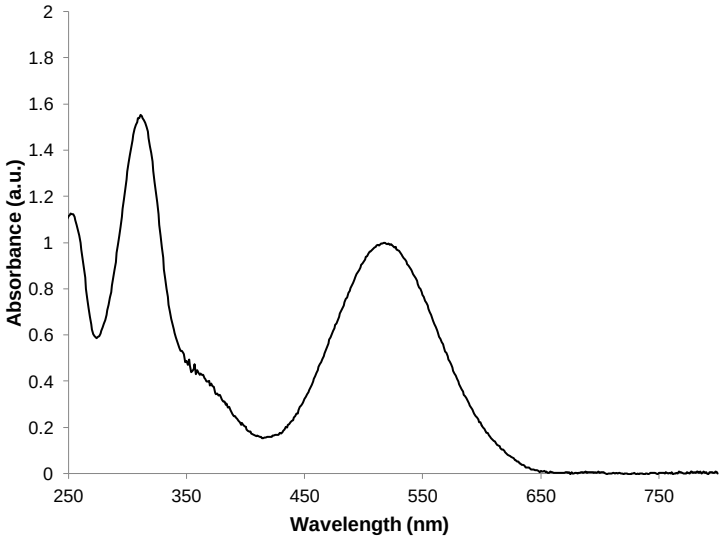

Fig. S15 UV-Vis absorption spectrum of BF_2 formazanate monomer **11** recorded in CH_2Cl_2.

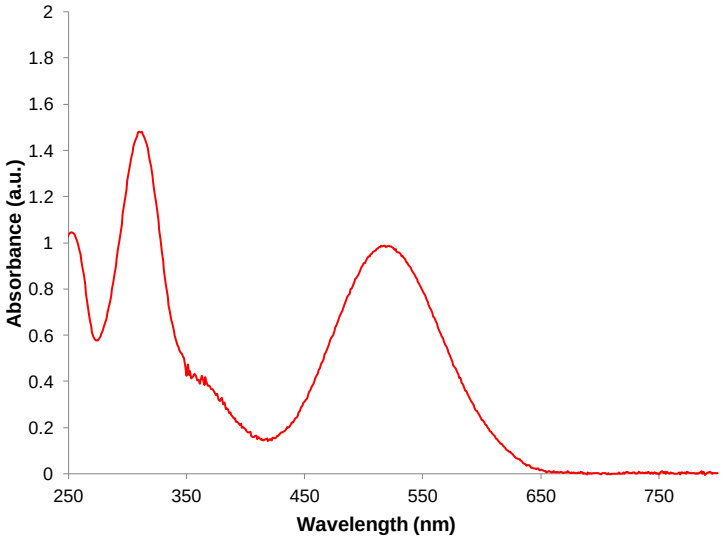

Fig. S16 UV-Vis absorption spectrum of BF_2 formazanate polymer **12** recorded in CH_2Cl_2.

Cyclic Voltammetry Data

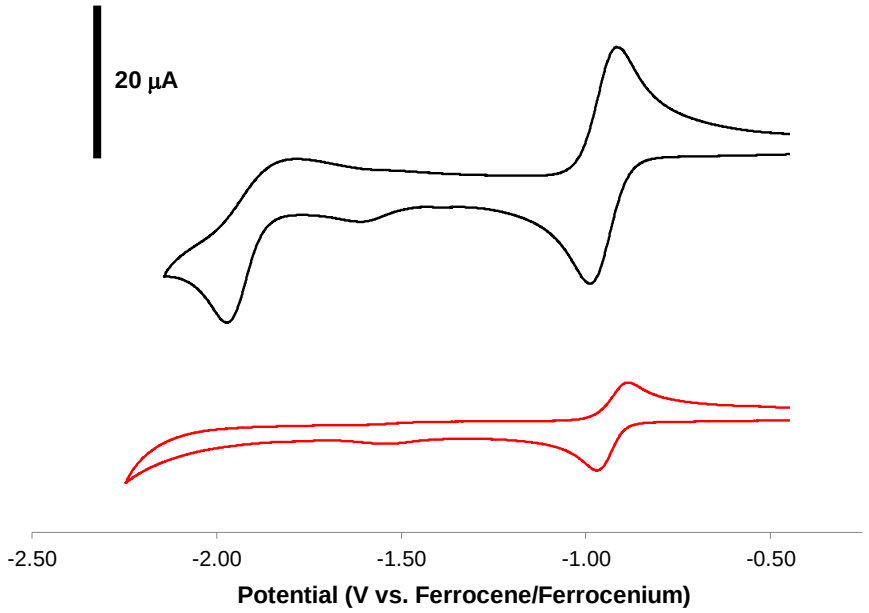

Fig. S17 Cyclic voltammograms for BF_2 formazanate monomer **11** (black line) and polymer **12** (red line) recorded in dry, degassed THF containing ~ 1 mM analyte and 0.1 M nBu$_4$NPF$_6$ at a scan rate of 250 mV s^{-1}.

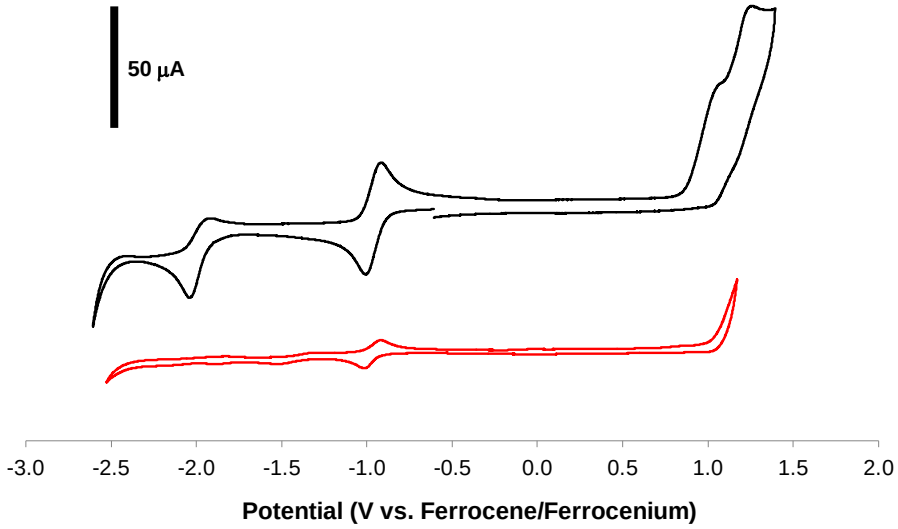

Fig. S18 Cyclic voltammograms for BF_2 formazanate monomer **11** (black line) and polymer **12** (red line) recorded in dry, degassed CH_2Cl_2 containing ~ 1 mM analyte and 0.1 M nBu$_4$NPF$_6$ at a scan rate of 250 mV s^{-1}.